Nuclear receptor Nur77 regulates immunomechanics of macrophages

Lith, S.C.; Evers, T.M.J.; Freire, B.M., Tiel, C.M. van; Vos, W.G.; Mashaghi, A.; Vries, C.J.M. de

European Journal of Cell Biology 103 (2024) 151419

Contents lists available at ScienceDirect

European Journal of Cell Biology

journal homepage: www.elsevier.com/locate/ejcb

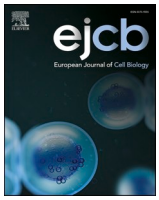

Nuclear receptor Nur77 regulates immunomechanics of macrophages

Sanne C. Lith [a,b,c,1], Tom M.J. Evers [d,1], Beatriz M. Freire [a,b,c], Claudia M. van Tiel [a,b,c], Winnie G. Vos [a,b,c], Alireza Mashaghi [d,2], Carlie J.M. de Vries [a,b,c,*,2]

[a] Amsterdam UMC location University of Amsterdam, Department of Medical Biochemistry, Amsterdam, The Netherlands
[b] Amsterdam Cardiovascular Sciences, University of Amsterdam, The Netherlands
[c] Amsterdam Institute for Immunology and Infectious diseases, University of Amsterdam, The Netherlands
[d] Medical Systems Biophysics and Bioengineering, Leiden Academic Centre for Drug Research, Faculty of Mathematics and Natural Sciences, Leiden University, Leiden, The Netherlands

ARTICLE INFO

Keywords:
Nur77
Immunomechanics
Actin cytoskeleton
Macrophage
Cellular stiffness

ABSTRACT

Nuclear receptor Nur77 plays a pivotal role in immune regulation across various tissues, influencing pro-inflammatory signaling pathways and cellular metabolism. While cellular mechanics have been implicated in inflammation, the contribution of Nur77 to these mechanical processes remains elusive. Macrophages exhibit remarkable plasticity in their morphology and mechanics, enabling them to adapt and execute essential inflammatory functions, such as navigating through inflamed tissue and pathogen engulfment. However, the precise regulatory mechanisms governing these dynamic changes in macrophage mechanics during inflammation remain poorly understood. To establish the potential correlation of Nur77 with cellular mechanics, we compared bone marrow-derived macrophages (BMDMs) from wild-type (WT) and Nur77-deficient (Nur77-KO) mice and employed cytoskeletal imaging, single-cell acoustic force spectroscopy (AFS), migration and phagocytosis assays, and RNA-sequencing. Our findings reveal that Nur77-KO BMDMs exhibit changes to their actin networks compared to WT BMDMs, which is associated with a stiffer and more rigid phenotype. Subsequent *in vitro* experiments validated our observations, showcasing that Nur77 deficiency leads to enhanced migration, reduced adhesion, and increased phagocytic activity. The transcriptomics data confirmed altered mechanics-related pathways in Nur77-deficient macrophage that are accompanied by a robust pro-inflammatory phenotype. Utilizing previously obtained ChIP-data, we revealed that Nur77 directly targets differentially expressed genes associated with cellular mechanics. In conclusion, while Nur77 is recognized for its role in reducing inflammation of macrophages by inhibiting the expression of pro-inflammatory genes, our study identifies a novel regulatory mechanism where Nur77 governs macrophage inflammation through the modulation of expression of genes involved in cellular mechanics. Our findings suggest that immune regulation by Nur77 may be partially mediated through alterations in cellular mechanics, highlighting a potential avenue for therapeutic targeting.

1. Introduction

Macrophages are innate immune cells with a crucial function in the body's defense against pathogens and infections. Upon recognition of a pathogen and in response to inflammatory signals, specific signaling pathways are initiated (Glass and Natoli, 2015; Liddiard and Taylor, 2015). While this inflammatory response of macrophages has been extensively studied and described, there are still unanswered questions regarding other properties that macrophages exhibit upon cell activation, such as their ability to alter cell mechanics. Macrophages are either tissue-resident cells or are derived from monocytes traveling through the bloodstream. Once monocytes adhere to activated vascular endothelial cells and translocate into the tissue, these cells differentiate into macrophages. Macrophages monitor tissue homeostasis, may expand in size, and are crucial in the phagocytosis of debris and pathogens (Medrano-Bosch et al., 2023). To carry out these functions, macrophages need

Abbreviations: Nur77, Nuclear Receptor 4A1; BMDM, Bone Marrow Derived Macrophages; AFS, Acoustic Force Spectroscopy; LPS, Lipopolysaccharides.

* Correspondence to: Amsterdam UMC, Meibergdreef 15, room K1-113, 1105AZ Amsterdam, The Netherlands.
E-mail addresses: a.mashaghi.tabari@lacdr.leidenuniv.nl (A. Mashaghi), c.j.devries@amsterdamumc.nl (C.J.M. de Vries).

[1] Shared first author
[2] Shared last author

https://doi.org/10.1016/j.ejcb.2024.151419
Received 17 January 2024; Received in revised form 17 April 2024; Accepted 8 May 2024
Available online 15 May 2024

to remodel their mechanical properties, a process largely dependent on the cell cytoskeletal network, and adhesiveness of the cell interface. Recently, we characterized the viscoelastic properties of monocytes at high resolution, demonstrating that these cellular properties are strongly regulated by cytokine stimulation (Evers et al., 2021). More specifically, the application of single-cell acoustic force spectroscopy (AFS) techniques revealed that these cells can adapt their mechanical properties in response to chemokines such as CCL2.

At present, the investigation of macrophage mechanics remains limited, but a complex interplay between macrophage phenotype and mechanical properties has been described. Specifically, pro-inflammatory (M1) and pro-resolution (M2) macrophages feature distinct viscoelastic properties, as revealed using single-cell optical tweezers and AFS approaches (Evers et al., 2022). In addition, it has been described that human macrophages exhibit increased actin polymerization in response to lipopolysaccharide (LPS) and interferon gamma (IFN-y) stimulation, which results in altered phagocytic function, adhesion, and migration capabilities (Bufi et al., 2015; Mcwhorter et al., 2016; Patel et al., 2012). Despite these advances, our understanding of the mechano-immunology of macrophages and its regulation is fundamentally incomplete, and the link between genomic and mechanical processes has not been fully explored.

The nuclear receptor Nur77 (gene name NR4A1) is a transcription factor that functions as a central regulator of innate and adaptive immune responses (Lith and de Vries, 2021). Nur77-deficient mice have been implicated in a variety of inflammation-driven pathologies, such as atherosclerosis, rheumatoid arthritis, and inflammatory bowel disease (Hamers et al., 2012; Hanna et al., 2012; Hu et al., 2014; Li et al., 2015; Shaked et al., 2015). Notably, macrophages are profoundly influenced by aberrant Nur77 activity in inflammatory disease. Upon stimulation by pro-inflammatory stimuli like LPS and tumor necrosis factor (TNF)-α, the expression of Nur77 increases in human and mouse macrophages (Bonta et al., 2006; Pei et al., 2005). Nur77 has been shown to restrict the macrophage inflammatory response via negative regulation of nuclear factor kappa B (NF-κB)-dependent cytokines (Li et al., 2015) and transcriptional reprogramming of mitochondrial metabolism (Koenis et al., 2018a). Additionally, studies have shown that a whole-body Nur77 deficiency or a macrophage-specific deletion in mice exacerbates atherosclerosis (Hamers et al., 2012; Hanna et al., 2012). Furthermore, Nur77-deficient mice exhibit increased macrophage infiltration and cytokine production in inflammatory bowel disease models (Wu et al., 2016). Nur77 deficiency also renders mice more susceptible to experimental autoimmune encephalomyelitis with a macrophage-specific deletion exacerbating disease severity through enhanced production of norepinephrine (Shaked et al., 2015). Furthermore, Nur77 is involved in regulating the differentiation of Ly6C^{lo} macrophages (Hanna et al., 2011).

So far, Nur77 has been described to be induced by stretching of vascular smooth muscle cells, however its effect on cellular mechanics has not been studied (De Waard et al., 2006). Yet, aberrant signaling of the androgen receptor, also a nuclear receptor, reprograms prostate cancer metabolism, thereby changing the mechanical phenotype of the cancerous cells (Chianese et al., 2022).

Here, we investigate the contribution of Nur77 to macrophage mechano-immunology. We achieved this by conducting a combination of biophysical, bioinformatic, and transcriptomics analysis of wild-type (WT) and Nur77-deficient murine bone marrow-derived macrophages (BMDMs). We characterized mechanical changes by quantifying the expression of cytoskeletal proteins, imaging the macrophages, and measuring the mechanical properties of these cells. The latter includes cell elasticity, phagocytic, and migratory activity of the cells, which are key to macrophage function in inflammation. Taken together, Nur77 affects both the inflammatory response of macrophages and the expression of mechanics-related genes. Our data contribute to further insights into the unexplored role of nuclear receptor signaling in the mechanical behavior of macrophages.

2. Results

2.1. Nur77 deficiency affects membrane organization and cell size

To study the involvement of the cytoskeleton in regulating cellular mechanics of macrophages after cell activation, we performed F-actin staining before and after LPS stimulation of bone marrow-derived macrophages (BMDMs) from wild-type (WT) C57/Bl6 and Nur77-deficient (Nur77-KO) mice (Fig. 1A). Nur77-KO BMDMs exhibit more disrupted F-actin localization compared to WT BMDMs. This was determined by quantification of the so-called ruffles, which are erect veils of membranes on the surface of cells that promote migration and respond to stimuli (Condon et al., 2020). The extent of ruffles was determined by quantification of the intensity of actin localized on the cell surface (Fig. 1B). An increase in ruffle formation suggests higher environmental sampling by phagocytes and has been associated with a more pro-inflammatory phenotype (Condon et al., 2020). Quantification of actin ruffles revealed that especially at the later time points of LPS stimulation, Nur77-KO BMDMs have more ruffles compared to WT BMDMs, indicating that the impact of Nur77 deficiency on the ruffle pattern changes over time. To further quantify changes in the morphological properties of the BMDMs, we measured the total cell surface area of both WT and Nur77-KO BMDMs and observed that the cell size of both increases in response to LPS stimulation. However, Nur77-KO BMDMs are smaller than WT BMDM and this difference in size is already noticeable before LPS stimulation. Furthermore, Nur77-KO BMDMs have a rounder appearance before LPS stimulation and expand less after LPS stimulation (Fig. 1C). In conclusion, Nur77 deficiency affects the mechanical properties of BMDMs especially after inflammatory stimulation as the cells have less ruffled areas of the cell membrane and their cell size is reduced.

2.2. Nur77 deficiency impacts the mechanical phenotype of macrophages

To execute their function, macrophages often need to control their morphology via the regulation of cellular mechanical properties. Thus, to see if Nur77 signaling contributes to this process, we analyzed the stiffness of the cells. WT and Nur77-KO BMDMs were subjected to acoustic force spectroscopy (AFS). This experimental setup, which combines optical microscopy and acoustic tweezing, allows for the quantification of cellular mechanical properties in high-throughput. WT and Nur77-KO BMDMs were mixed with silica microspheres and injected into AFS microfluidic chips. The cells were then allowed to adhere to the bottom of the chips and cultured overnight at a slow flow rate. Notably, both WT and Nur77-KO BMDMs spontaneously seized the silica microspheres on top without engulfing them (Supplemental Fig. S1A). By analyzing the response of the cells to the applied acoustic forces, we observed that the Nur77-KO macrophages exhibit significantly higher elastic modulus at basal conditions, as compared to the WT BMDMs (Fig. 2A). It is noteworthy to mention that the elastic modulus of WT macrophages significantly increases upon LPS exposure, as in agreement with existing literature (Bufi et al., 2015; Patel et al., 2012). The elastic modulus of LPS-treated Nur77-KO is also higher than the elastic modulus of LPS-treated WT macrophages.

2.3. Nur77 affects macrophage migration, cell adhesion, and phagocytic capacity

We next asked whether the observed Nur77-mediated mechanical, morphological, and cytoskeletal alterations are associated with changes in macrophage migratory and phagocytic capacity. Single-cell migration was monitored overnight under LPS stimulation showing that Nur77-KO BMDMs are more migratory than WT BMDMs when stimulated (Fig. 2B). Detailed analyses demonstrated that the velocity and directness of the cells are increased in Nur77-KO compared to WT BMDMs only when stimulated with LPS (Fig. 2C-D).

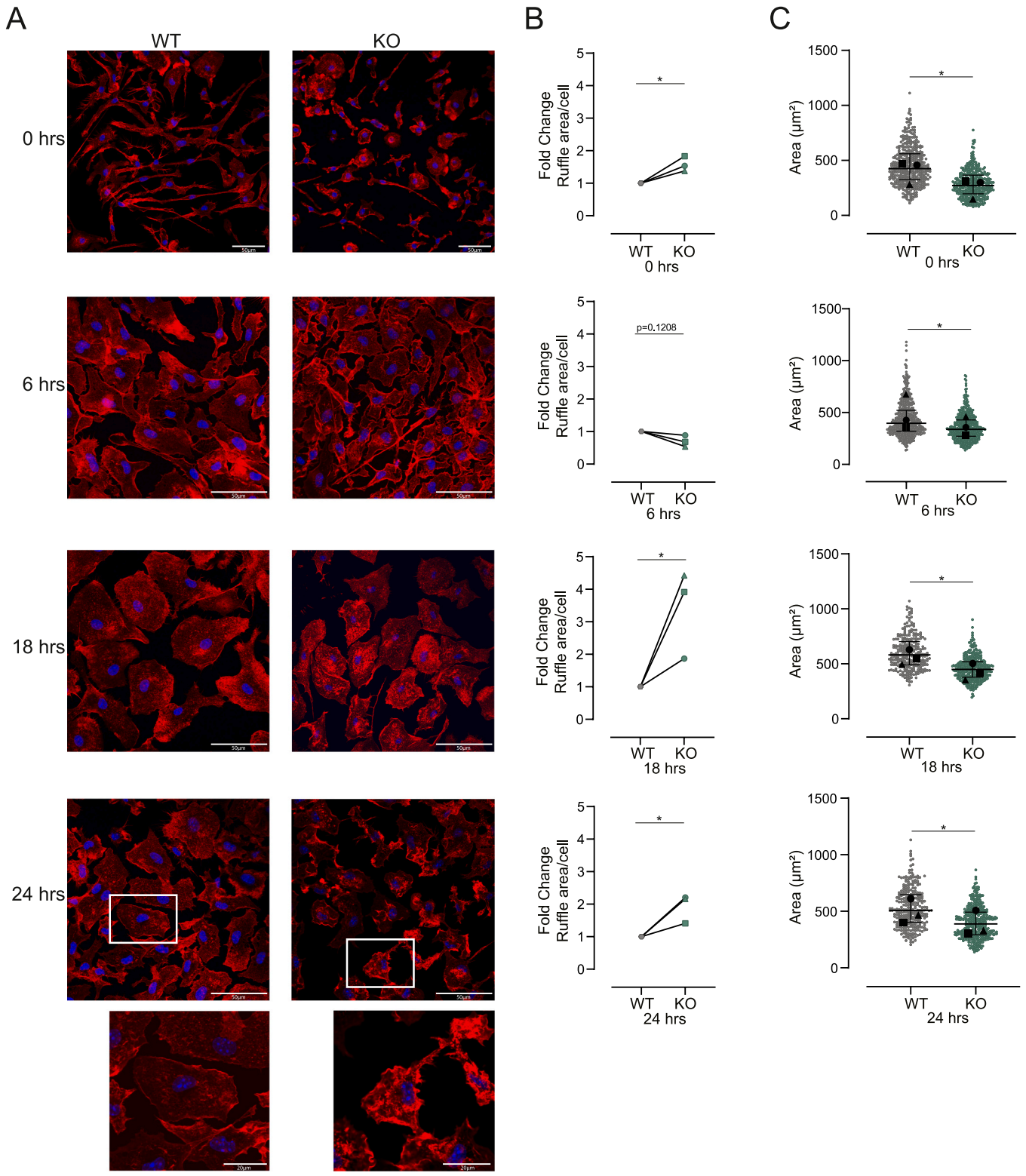

Fig. 1. Microscopic analysis unveils the role of Nur77 in macrophage size and membrane formation. A: Representative immunofluorescent images of WT and Nur77-KO BMDMs stained for F-actin (red) and nuclei (blue) stimulated with LPS for 0, 6, 18, or 24 hrs. Corresponding close-up images are shown for the cells after 24 hrs of stimulation. Scale bars, 10 µm. B: Quantification of the ruffled edges of WT and Nur77-KO BMDMs at corresponding time points. The total area of ruffled edges per image was corrected for total cell number and then normalized to the corresponding WT mice. Each symbol represents a biological replicate (n = 3 mice) and ratio paired t-test was performed. C: Quantification of single cell area in μm^2 of WT and Nur77-KO BMDMs at corresponding time points. Small dots represent single cells, large symbols are medians of each biological replicate. The lines in the plot display the quartiles and median of all data points (n = 3 mice). A ratio paired t-test was performed. 0 hrs, 410 WT cells and 367 KO cells; 6 hrs, 516 WT cells and 506 KO cells; 18 hrs, 272 WT cells and 340 KO cells; 24 hrs, 281 WT cells and 375 KO cells. *P<0.05.

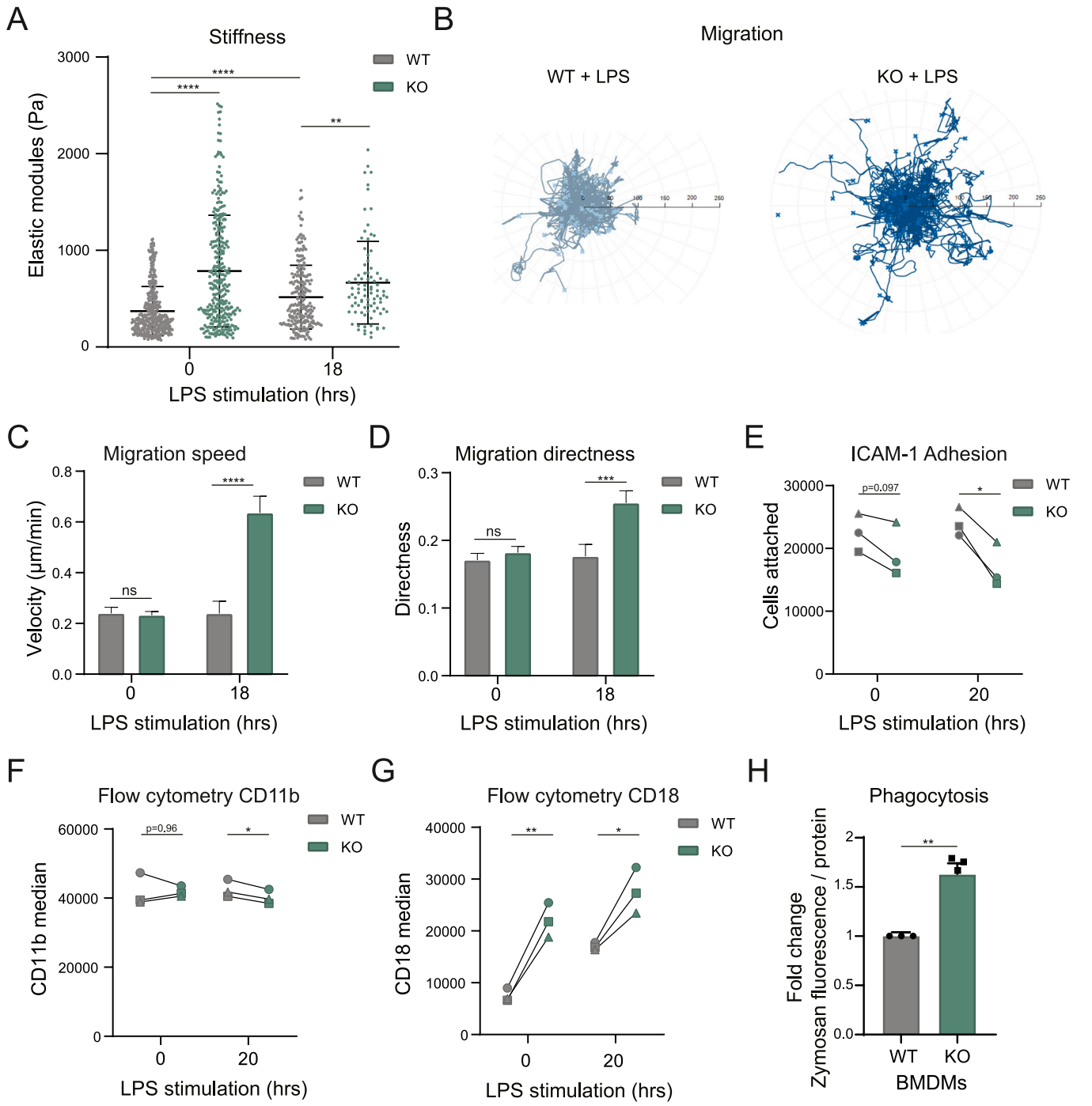

Fig. 2. Nur77 regulates mechanical properties such as cellular stiffness, macrophage migration, adhesion, integrin expression, and phagocytosis. A: Probing WT and Nur77-KO BMDM mechanical properties using acoustic force spectroscopy (AFS). The stiffness measured in elastic modulus (Pa) of WT and Nur77-KO BMDMs before and after LPS treatment was determined. Each data point represents a single cell. Mann–Whitney test, 0 hrs) n=360 WT; n=309 KO, 18 hrs) n=227 WT; n=87 KO. Data from n = 3 mice was analyzed together. B: Migration pattern after overnight migration of WT and Nur77-KO BMDMs after 18 hrs LPS pre-incubation. Each point represents a single cell. C-D: Quantification of migration velocity in µm/min and directness for WT and Nur77-KO BMDMs. Two-way ANOVA, 0 hrs) n= 724 WT; n= 508, 18 hrs) n= 135 WT; n= 226. E: Dot plot showing the mean amount of WT and Nur77-KO BMDMs adhered to ICAM-1 after 0 or 20 hrs of LPS stimulation quantified after Hoechst staining. Each symbol represents a biological replicate (n = 3 mice) and a multiple paired t-test was performed. F-G: CD11b or CD18 median expression was determined by flow cytometry for WT and Nur77-KO BMDMs left untreated and treated with LPS for 20 hrs. Each symbol represents a biological replicate (n = 3 mice) and multiple paired t-test was performed. H: Phagocytosis of WT and Nur77-KO BMDMs was quantified with Zymosan Fluorescence kit and expressed as a fold change of Nur77-KO over WT BMDMs. Ratio paired t-test was performed on mean fold change per biological replicate (symbols). For (A), data are shown as mean±SD (error bars) or for (C,D,H) mean±SEM (error bars), ns non-significant; *P<0.05;**P<0.01;***P<0.001; ****P<0.0001.

To gain a better understanding of the enhanced migratory capacity of Nur77-deficient BMDMs, we hypothesized that interfacial adhesion may be decreased in KO cells. To test this, WT and Nur77-deficient BMDMs were allowed to adhere to ICAM-1 coated plates. Nur77-KO BMDMs exhibit a decreased adhesion to ICAM-1 compared to WT BMDMs after stimulation (Fig. 2E). Transmembrane integrins play a crucial role in the adhesion of macrophages, therefore we further analyzed the expression of such proteins (Schittenhelm et al., 2017). The most critical integrin for macrophage adhesion and migration is CD11b/CD18 (also known as Mac-1), which is a heterodimer of the subunits αM (CD11b, ITGAM) and β2 (CD18). In line with our adhesion experiments, flow-cytometry analyses revealed that after LPS stimulation CD11b protein expression on the cell surface of Nur77-KO BMDMs is lower compared to the expression on WT BMDMs (Fig. 2F). Protein expression of CD18 on the cell surface is, however, upregulated (Fig. 2G). Since the adherence of Nur77-KO BMDMs to ICAM-1 is reduced, one may propose that the expression of CD11b is rate-limiting and/or that even though CD18 protein expression is elevated, the protein is not fully functionally active. At present, no antibodies are available to determine the open (active) conformation of murine CD11b/CD18.

Phagocytosis is yet another process that requires tight regulation of the cytoskeleton and is crucial for BMDM function (Dupuy and Caron, 2008). To study this process, BMDMs were incubated with fluorescent Zymosan particles and uptake was measured by flow cytometry. Notably, Nur77-KO BMDMs showed more phagocytosis compared to WT BMDMs (Fig. 2H).

In conclusion, after LPS stimulation, cell migration is increased and adhesion is reduced in Nur77-KO BMDMs compared to WT BMDMs, which is in line with a lower abundance of integrin CD11b, while the phagocytic capacity of Nur77-deficient cells is increased.

2.4. Transcriptome analysis of Nur77-deficient and WT BMDMs after LPS stimulation

To investigate the role of Nur77 in the regulation of macrophage function under inflammatory conditions in further detail, we performed transcriptomic analyses. In WT BMDMs, Nur77 mRNA expression shows a rapid and transient response to LPS stimulation, with maximum expression at 1 hr, and already after 2 hrs there is again almost no Nur77 mRNA detectable (Fig. 3A). Endogenous Nur77 protein expression in macrophages has been described to maintain for at least 18 hrs (Koenis et al., 2018a). Next, we performed, to our knowledge for the first time, extensive RNA sequencing (RNA-seq) for WT and Nur77-deficient BMDMs after short (4 hrs) or prolonged (18 hrs) LPS activation. As expected, we observed substantial differential gene regulation when comparing Nur77-KO with WT BMDMs. Notably, the impact of Nur77 deficiency on gene transcription was most pronounced at the later time point of LPS stimulation (Fig. 3B). To further analyze the RNA-seq data, we organized the data in a heatmap with unbiased ordering in 8 clusters of genes with similar expression patterns affected by deficiency of Nur77 and 4 hrs or 18 hrs of LPS activation (Fig. 3C).

To reveal the impact of Nur77 deficiency on gene expression in the context of macrophage activation by LPS, we performed pathway analyses at 18 hrs of LPS stimulation (Fig. 3D). The positive association of Nur77 deficiency with inflammatory pathways is very strong, which is illustrated by the fact that 6 out of 10 of the pathways with the strongest effect on their normalized enrichment scores concern inflammatory signaling (Fig. 3D). In addition, we observed upregulation of hypoxia-related pathways in Nur77-KO BMDMs, as well as reduced oxidative phosphorylation, consistent with the previously described role of Nur77 in macrophage metabolism (Koenis et al., 2018a). A more detailed representation of the different pathways with the running enrichment scores over the position in the ranked list of genes further substantiates the relevance of these pathways in Nur77-regulated cellular signaling (Supplemental Figure S2A). The top 40 genes of the rank list belonging to the HALLMARK_Inflammatory_Pathway are listed in a separate heatmap with the gene names indicated. In this list of genes multiple cytokines, NF-kB-related genes, and hypoxia-related factors are present (Supplemental Figure S2B).

Next, pathway analysis was conducted on all 8 clusters presented in the heatmap, revealing different aspects of Nur77 function in activated macrophages (Fig. 3C; Supplemental Figure S3A). Consistent with the observations made for the entire dataset as described above, the genes in clusters 3, 4, 5, and 7 all affiliate with inflammatory pathways. Regulation of the genes in clusters 1, 2, and most specifically and strongly, in cluster 6, relate to cellular proliferation, cell division, the cell cycle, and nucleotide metabolism, with the strongest effect of Nur77-deficiency at the onset of the experiment, so before LPS stimulation.

Most interestingly for this study, and related to the observed differences in cellular mechanics of Nur77-KO compared to WT BMDMs, the gene set in cluster 8 exhibits a strong association with extracellular matrix aspects, such as collagen and elastic fiber formation, as well as with cell adhesion, contraction, motility, and migration (Fig. 3E). Given that these specific pathways are strongly related to the migratory and phagocytotic capacity of cells, involving movement and mechanical cellular deformation, we considered that the reorganization of their cytoskeleton may be affected.

Collectively, these transcriptomic data underscore the prominent role that Nur77 has in the later stage of inflammation in macrophages, concerning the resolution phase in which the inflammatory response is put to an end to prevent excessive local tissue damage. Most relevant for our current study, we discovered that Nur77 deficiency regulates the expression of a group of genes related to cellular mechanics.

2.5. Nur77 deficiency leads to highly adaptable regulation of mechanic-related genes

To further investigate the potential role of Nur77 in the mechanical properties of macrophages, we analyzed the up- and downregulated genes from the RNA-sequencing in response to LPS stimulation separately. Splitting the dataset into up- and downregulated genes revealed that the majority of differential regulation occurred at 18 hrs of LPS stimulation, reinforcing the notion that Nur77 deficiency primarily dysregulates genes during the resolution phase of the inflammatory response (Fig. 4A-B). In addition, after 18 hrs of LPS stimulation, more genes are upregulated than downregulated in Nur77-KO BMDMs compared to WT BMDMs, suggesting that Nur77 has mostly a repressive effect on transcription of the genome in macrophages.

When studying the associated pathways of the separate lists of up- and downregulated genes by gene-set enrichment analysis (GSEA), the cytoskeleton-related pathways showed up in both the upregulated and downregulated gene sets, depending on the time points of LPS stimulation. To further delineate this observation, we analyzed these pathways in more detail and observed that at 0 hrs of LPS stimulation, genes affiliated with the cytoskeleton pathway are mostly downregulated. However, after 4 hrs of LPS stimulation, the contribution of up- and downregulated genes in this pathway is similar, followed by a remarkable upregulation of these genes after 18 hrs of LPS stimulation. This pattern was observed for all pathways associated with the cytoskeleton, including '*Cytoskeleton*', '*Cytoskeletal Part*', '*Cytoskeleton Organization*', '*Regulation of Cytoskeleton Organization*', and '*Microtubule Cytoskeleton*' (Fig. 4C), and with actin associated pathways (Supplemental data Fig. S4A). This pattern is not observed for genes involved in inflammatory pathways like '*Cellular Response to Cytokine Stimulus*' or genes related to '*Oxidation Reduction Process*' (Supplemental data Fig. S4B). Overall, the regulation of Nur77 on cytoskeleton-related pathways appears to change at different stages of inflammatory stimuli.

To determine whether a specific set of genes exhibits a reversal of their expression pattern upon Nur77 deficiency or whether certain groups of genes are either downregulated or upregulated, all the hits of the GSEA of the '*Cytoskeleton Pathway*' were listed at the individual time points; 0, 4, and 18 hrs of LPS stimulation (Supplemental Figure S4C).

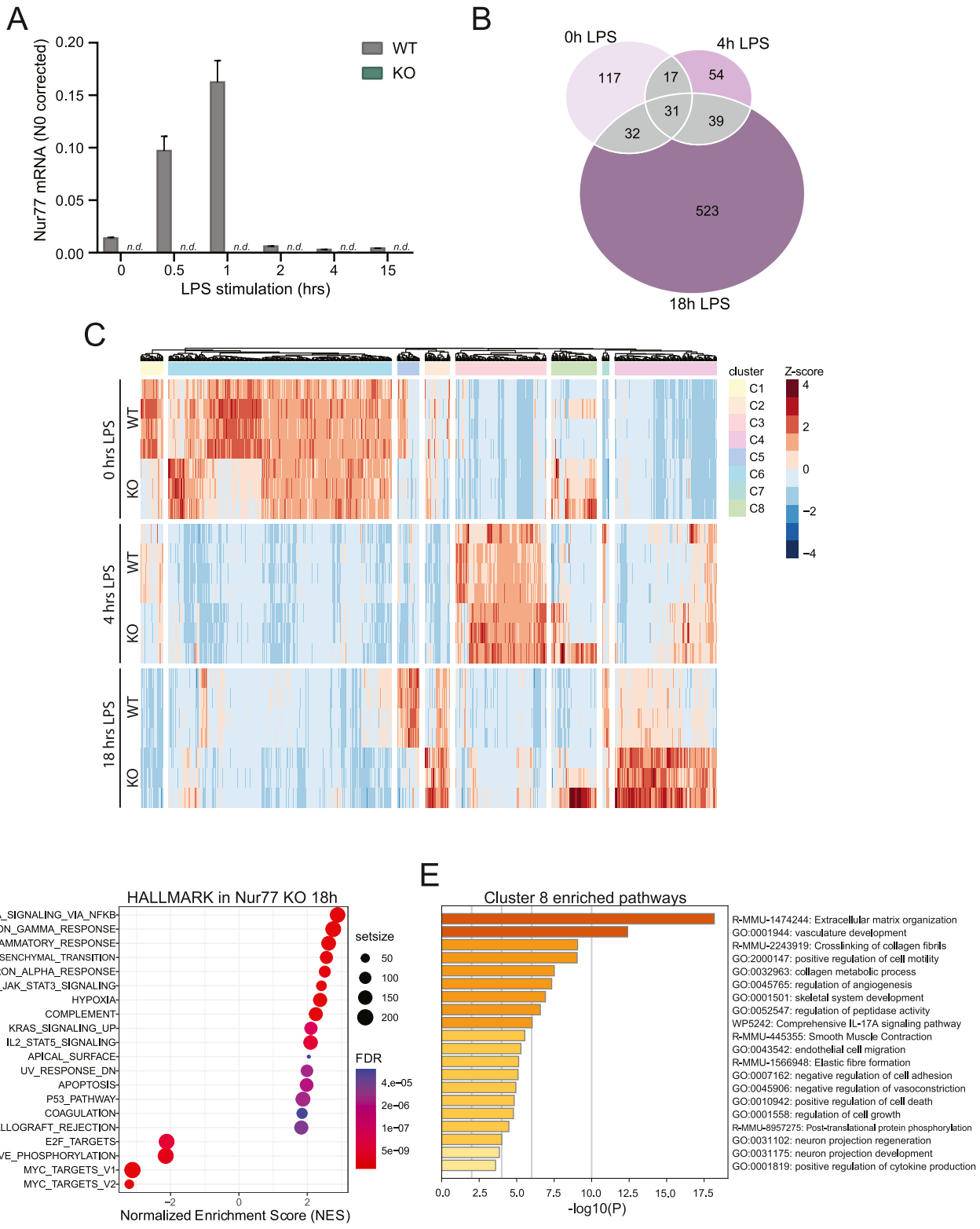

Fig. 3. Transcriptomics of WT and Nur77-KO BMDMs shows differentially regulated gene clusters implicating a role for Nur77 in cellular inflammation and mechanics in macrophages after LPS stimulation. A: Nur77 gene expression in WT and Nur77-KO BMDMs left untreated or treated with LPS for the indicated times, biological replicates n = 2 mice, mean±SEM, *n.d.*= not detected. B) Venn Diagram of differentially expressed genes found in RNA-sequencing at the indicated time points of LPS treatment in WT and Nur77-KO BMDMs with a significant change in expression level ($P<0.05$) and a >2-fold change in expression. C: Hierarchical clustering of genes and z-score heatmap of differentially expressed genes between WT and Nur77-KO BMDMs. Color annotation represents the unbiased clustering of 8 groups. Different time points of LPS treatment are shown in purple. D: Most enriched HALLMARK gene sets in Nur77-KO BMDMs compared to WT treated with LPS for 18 hrs. E: Top enriched pathways in Nur77-KO BMDMs compared to WT for genes of cluster 8 in the RNA-sequencing dataset obtained from Metascape. All RNA-seq data was performed on n = 4 WT mice and n = 3 KO mice.

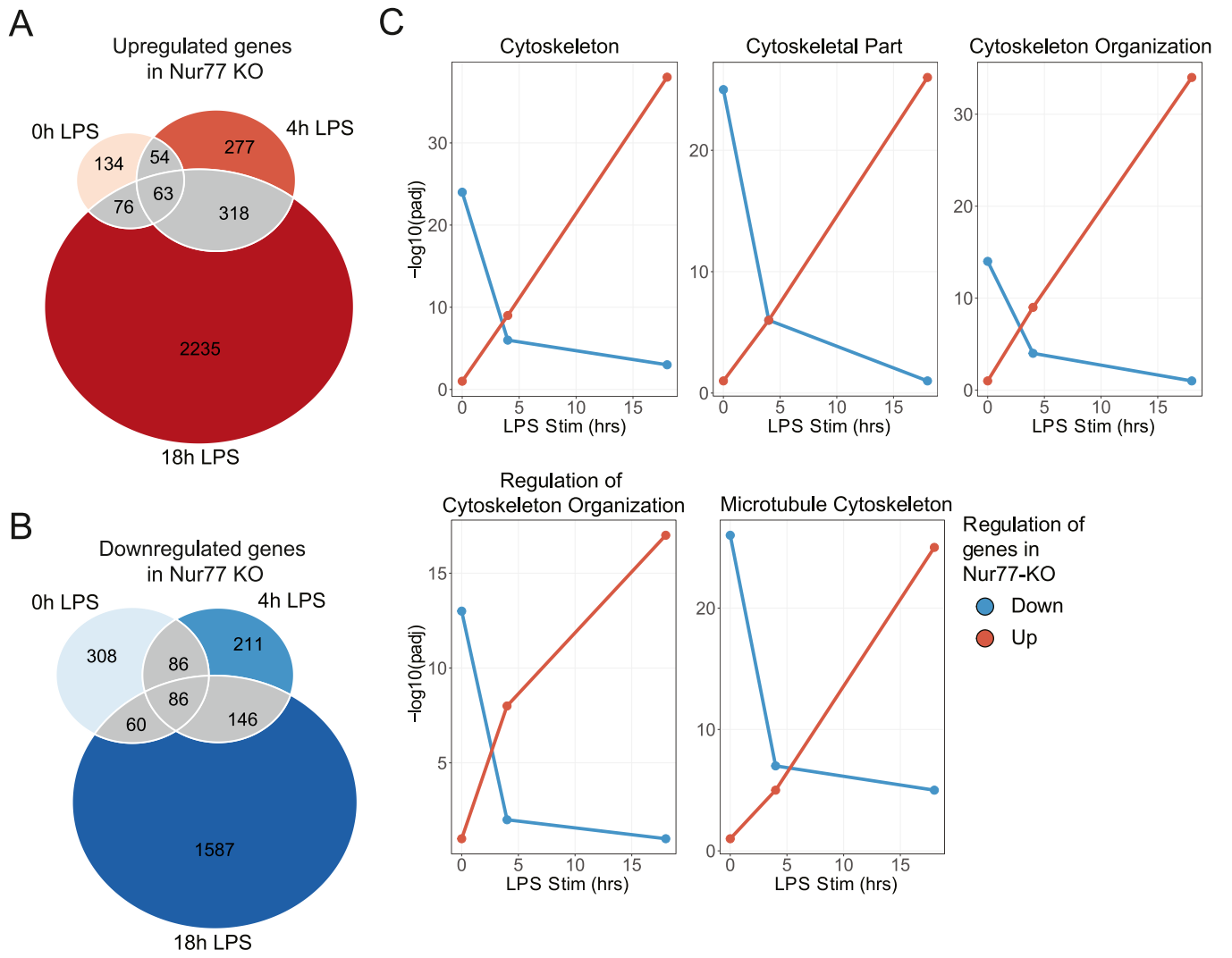

Fig. 4. The regulation of cytoskeletal pathways in Nur77-KO BMDMs is highly dependent on the time of LPS stimulation. A-B: Venn Diagram in red of differentially upregulated genes (A) and in blue of differentially downregulated genes (B) in Nur77-KO compared to WT BMDMs in the RNA-sequencing dataset with a P-value <0.1 and a fold-change >1 for LPS treatment at the indicated time points. C: For distinct mechanic-pathways from GSEA the P-values are indicated at different time points of LPS treatment. The blue lines represent how significantly the indicated pathways are associated with downregulated genes and the red line represents how significantly the indicated pathways are associated with upregulated genes in Nur77-KO compared to WT BMDMs. Every dot represents one time point. All RNA-seq data was performed on n = 4 WT mice and n = 3 KO mice.

Next, we examined the expression profile of all genes with a significant difference between WT and Nur77-KO macrophages over time. Genes such as *Cep250, Kif23, Nek2*, and *Tpm4* (marked in red) show a different regulation over time; in unstimulated macrophages, their expression is lower compared to WT macrophages, and at 18 hrs their expression is increased in Nur77-KO macrophages compared to WT macrophages.

Taken together, these results indicate a diverse regulation of the cytoskeleton in BMDMs following stimulation and highlight the impact of Nur77 at these distinct stages of inflammatory stimulation. Given that macrophages initially contract in response to inflammatory stimuli and then expand and migrate, these transcriptomics data support a highly adaptable regulatory mechanism for the cytoskeleton in these cells (Jain et al., 2019; Ronzier et al., 2022).

2.6. *Nur77 directly regulates the transcription and expression of mechanic-related genes*

To explore whether the transcription factor Nur77 has a direct role in regulating the expression of genes with a crucial function in the cellular mechanics of macrophages, we selected signature genes derived from above mentioned GO pathways. We presented the expression profile of these genes in a heatmap (Fig. 5A). Next, we determined whether these genes contain a Nur77-specific response element (AAAGGTCA) within 5 kilobases (kB) from the transcription start site (TSS). In the promoter regions of 42% of these genes, we detected a DNA sequence with at least 80% homology with the Nur77-response element (genes indicated in green; Fig. 5A). To further substantiate the potential interaction of Nur77 with these elements, we explored our previously obtained Nur77 ChIP-seq datasets in RAW264.7 mouse macrophage cells and C2C12 mouse myoblast cells overexpressing Nur77 (Koenis et al., 2018a). For 11 out of the 14 genes indicated in green in the heatmap, DNA binding of Nur77 was observed in this ChIP-seq dataset. As an example, the ChIP-seq results for *Itgb2* and *Capza2* are shown with the Nur77 response element in the peaks indicated (Fig. 5B). Remarkably for *Itgb2*, the binding of Nur77 at these loci appears to be cell-type specific, as no or less binding is observed in C2C12 cells. In contrast, the binding of Nur77 to the *Capza2* promoter seems to be conserved between these cell types. Finally, protein levels of Itgb2 and Capza2 were determined by Western blot analyses to prove that not only mRNA but also protein expression is lower in Nur77-KO compared to WT BMDMs (Fig. 5C-D).

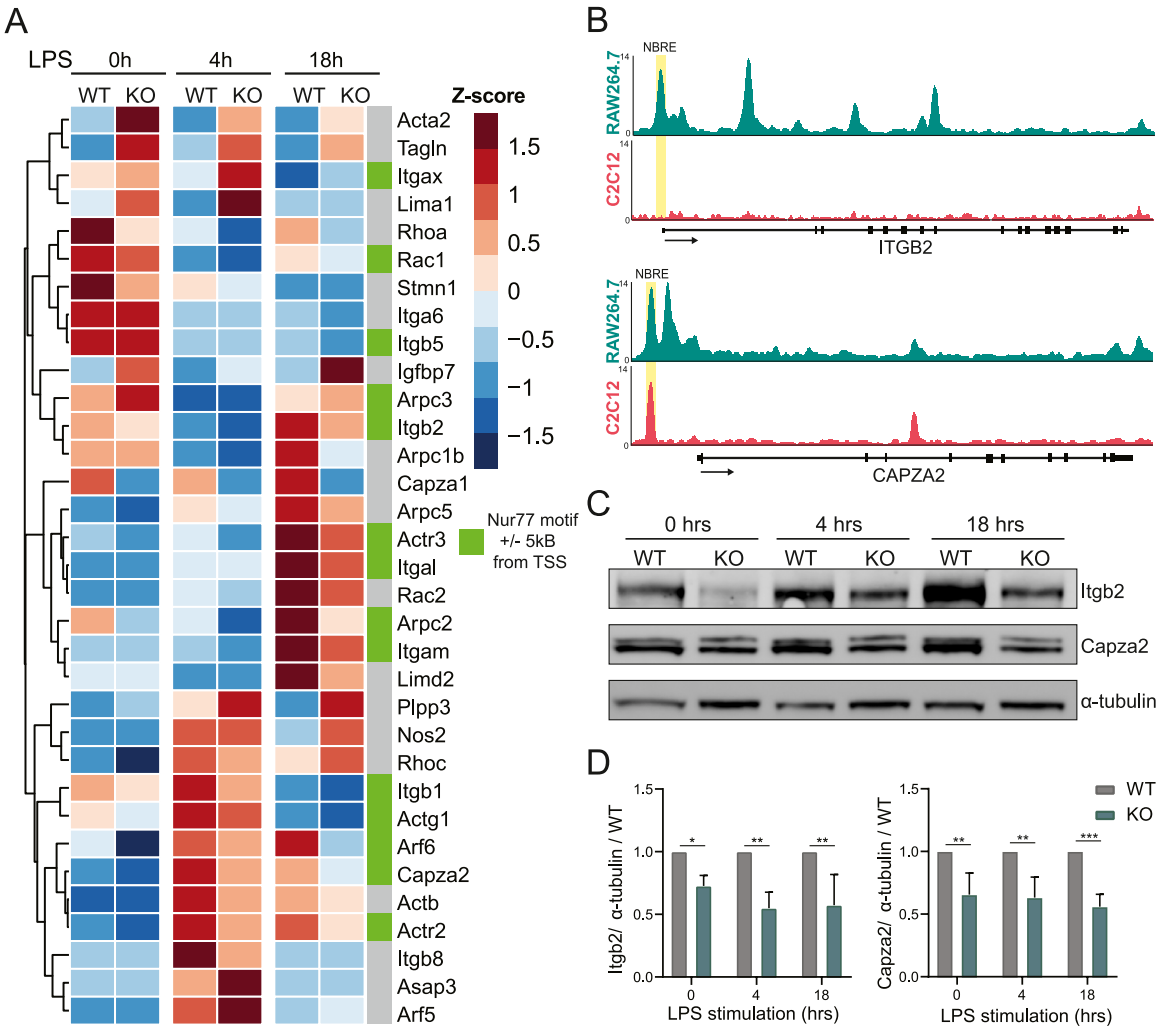

Fig. 5. The combination of transcriptome and DNA-binding profiles of Nur77 imply the direct regulation of Nur77 on important mechanic-related genes. A: Hierarchical clustering of mechanic genes in Z-score heatmap of WT and Nur77-KO BMDMs based on RNA-sequencing data at the indicated time points of LPS stimulation. Genes written in green contain a Nur77 motif (NBRE) at +/- 5kB from the TSS of that gene. B: The previously obtained Nur77 ChIP-seq dataset was used to determine Nur77 DNA binding in RAW264.7 (turquoise) and C2C12 (red) cells. Example snapshots are presented of Nur77 ChIP-seq data for ITGB2 and CAPZA2. Yellow boxes indicate the presence of an NBRE motif. The Y-axis shows the ChIP-seq signal in fragments per kB per million reads mapped. C: Representative western blot for Itgb2 and Capza2 protein in WT and Nur77-KO BMDMs treated with LPS for the indicated time points; α-tubulin was used as loading control. D: Fold change quantification of independent Western blot experiments (n = 3 mice) as shown in panel C. The fold change is normalized to α-tubulin and the WT from each separate time point of LPS stimulation. All RNA-seq data performed on n = 4 WT mice and n = 3 KO mice. Graphs represent mean ± SD (error bars); *P<0.05;** P<0.01;***P<0.001.

Taken together, our transcriptomic data support a role for LPS stimulation and Nur77 in cellular mechanics, involving changes in the plasticity of the cytoskeleton that affect cellular stiffness, migration, adhesion, and phagocytosis. Furthermore, we propose that the changes in cellular mechanics are not only a secondary effect of the pro-inflammatory phenotype of Nur77-KO BMDMs, but as our data suggest a direct effect of Nur77 functioning as a transcription factor binding immunomechanic-related target genes to regulate their transcription and expression.

3. Discussion

In the last decade, extensive insight has been gained concerning the heterogeneity of macrophage phenotypes, emphasizing these cells' plasticity and remarkably diverse functions. Macrophages strongly respond to environmental signals such as secreted cytokines and differentiation factors (Liddiard and Taylor, 2015). Only recently, alterations in extracellular matrix stiffness and spatial constraints have been shown to exert a discernible impact on the polarization of macrophages (Chen et al., 2020; Jain et al., 2019; Okamoto et al., 2018). A mechanical cue in the extracellular environment can induce a multi-faceted sequence of events in macrophages; adaptation of morphological characteristics, cytoskeletal modifications, altered gene expression, or vice versa, resulting in differentiation of cellular function. In an inflammatory setting, macrophages start migration and phagocytosis in response to extracellular cues, requiring drastic cytoskeleton rearrangement (Bufi et al., 2015; Ronzier et al., 2022). While the precise pathways governing the interplay between inflammation and cell mechanics remain elusive, noticeable alterations collectively underscore a tightly orchestrated regulatory mechanism (Atcha et al., 2021; Dutta et al., 2020). In the current study, we introduce the transcription factor Nur77 as a contributor to immunomechanics of macrophages in addition to its well-known function as an inhibitor of the inflammatory response of macrophages (Lith and de Vries, 2021). Our findings demonstrate that Nur77 deficiency alters primary murine macrophages' elastic modulus, reduces cell size, and enhances phagocytosis. In line with these observations, we observed reduced adhesion and enhanced migration of LPS-stimulated macrophages in the absence of Nur77 signaling.

Furthermore, our transcriptomic analyses revealed remarkable changes in the expression of key mechanical signature genes, which may be directly regulated by Nur77.

The anti-inflammatory impact of Nur77 in macrophages encompasses multiple aspects, among which the direct attenuation of gene expression of inflammatory cytokines, as well as the inhibition of pro-inflammatory transcription factors like NFκB through trans-repression (Hanna et al., 2012). Furthermore, we have previously demonstrated that Nur77 inhibits the formation of the pro-inflammatory metabolite succinate by interfering with mitochondrial metabolism (Koenis et al., 2018a). Our RNA-seq data show that Nur77-KO BMDMs are, as expected, more pro-inflammatory in response to LPS compared to WT BMDMs (Fig. 4A). Previously, pro-inflammatory macrophages have been associated with increased intrinsic cellular stiffness, enhanced phagocytic activity, more ruffled membrane edges, and augmented migratory capability (Condon et al., 2020; Patel et al., 2012). In the current study, we observed similar mechanical changes when comparing WT and Nur77-KO BMDMs, raising the question of whether these mechanical changes are a secondary effect of the pro-inflammatory phenotype of Nur77-deficient BMDMs. It should be noted, however, that Nur77-KO BMDMs already exhibit alterations in cellular mechanics and gene expression before stimulation with LPS. Moreover, our ChIP-seq data revealed that Nur77 directly binds genes encoding proteins associated with cellular mechanic properties. Based on these observations, we propose that modulation of the mechanical characteristics of macrophages is an additional mechanism through which Nur77 restrains inflammation.

We observed that Nur77-KO BMDMs exhibit reduced adhesion to ICAM-1 compared to WT BMDMs. The integrins CD11b and CD18 are known to bind ICAM-1 (Ross and Vetvicka, 1993; Ruoslahti, 1991). Therefore, we expected to observe less expression of these integrin subunits in Nur77-KO BMDMs. For CD11b, the RNA-seq data indeed revealed a reduction in expression in Nur77-deficient BMDMs, which also results in reduced protein exposure on the cell surface. Intriguingly, despite lower CD18 mRNA expression, as well as reduced CD18 protein expression in total cell lysates, CD18 exposure on the cell surface is higher for Nur77-KO BMDMs compared to WT BMDMs. These data highlight the importance to assess whether CD11b/CD18 has its active or 'open' conformation. Unlike the human situation, no mouse-specific antibodies have been described that specifically detect the active conformation of CD11b/CD18, which is crucial to elucidate this complex issue. Taken together, although CD18 surface expression was increased, the observed lowered adhesion may indicate reduced functionality of CD11b/CD18 integrins.

The simultaneous presence of dysfunctional CD11b/CD18 and heightened phagocytosis may appear contradictory (Sun et al., 2021). This apparent discrepancy may be attributed to the involvement of various other cell surface proteins, such as the mannose receptor and dectin-1 receptor, in the internalization of Zymosan particles (Underhill and Ozinsky, 2002). Moreover, other proteins, like PI3Kγ, Kindlin-3, Arp2/3, and Rho GTPases, have been described to be crucial for phagocytosis and the mRNA expression of some of these are actually changed in Nur77-KO BMDMs (Fig. 5A) (Bouti et al., 2021; Liu et al., 2020; Mao and Finnemann, 2015).

One of the limitations of our study is the lack of *in vivo* data to confirm macrophage mechanic phenotypes in an inflammatory disease-related setting. In previous studies, we have shown in mice that thioglycollate-induced migration of inflammatory cells to the peritoneal cavity is higher in Nur77-deficient than in WT-type mice (Hamers et al., 2012). More specifically, both B cell and macrophage influx was increased (Hamers et al., 2012; Morrison et al., 2014). It is conceivable that cellular mechanics and inflammation reciprocally constrain or assist each other, given their interdependence (Mukhopadhyay, 2023). Moreover, we show that the impact of Nur77 deficiency on mechanical alterations changes in response to LPS stimulation. This aligns with the intricate role Nur77 has in inflammation, being an early-response gene that contrastingly influences especially the resolution phase of macrophage activation. Another limitation is that we did not perform rescue studies in the Nur77-deficient BMDMs to establish that changed cellular mechanics could be reversed.

Previously, we analyzed the transcriptome of primary Nur77-deficient macrophages by microarray analyses and observed changes in the expression of genes involved in extracellular matrix synthesis and degradation (Hamers et al., 2016). It should be noted however, that at that time we used the so-called classical Nur77-deficient mouse model that had been generated through homologous recombination, which we demonstrated to express high levels of a truncated Nur77-variant (Koenis et al., 2018b). This truncated Nur77-variant has significant adverse effects on the inflammatory status of the liver and spleen in aging mice. In the current study, we applied the Cre-Lox system-derived Nur77-deficient mouse line, in which the Nur77 gene has been deleted completely. We propose that the current data provide therefore more reliable insight on the impact of Nur77 deficiency in macrophage phenotype and function.

The current RNA-sequencing data allow for a more in-depth analysis of Nur77-regulated gene expression, and we have extended our transcriptome studies with analyses of LPS-stimulated macrophages. We observed a remarkable regulation of cellular mechanics-related genes being dysregulated upon Nur77 deficiency. Of particular note is the changed expression of actin-related proteins (*Actr3*, *Actr2*) and actin-related protein complex subunits (*Arpc3*, *Arpc1b*, *Arpc5*, *Arpc2*) in Nur77-KO BMDMs (Fig. 5A). These genes are well-known for their influence on macrophage mechanics (Ronzier et al., 2022; Rotty et al., 2017). Additionally, RhoGTPases such as *Rac1/2* and *RhoA/C* show changed expression and are recognized for their role in modulating adhesion and phagocytosis of macrophages (Allen et al., 1997). More specifically, some of those genes showed strong upregulation, whereas others involved in cellular mechanics were downregulated in response to LPS, with the strongest effects after prolonged activation (18 hrs). The mere fact that Nur77-motifs are localized in the genome close to the TSS of the genes with a changed expression upon Nur77 deficiency supports our hypothesis that Nur77 directly regulates their expression; *Actg*, *Actr2*, *Actr3*, *Arf6*, *Arpc3*, *Capza2*, *Itgb1*, *Itgb2*, *Itgb5*, *ItgaI*, *Itgax*, and *Rac1*. This hypothesis is further substantiated by previous ChIP data obtained in RAW264.7 macrophage cells overexpressing Nur77 confirming the direct binding of Nur77 to the promoter of several of these genes (Koenis et al., 2018a).

Nur77, belonging to the superfamily of nuclear receptors, is categorized as an 'orphan receptor' due to the absence of an identified physiological ligand which may be due to the fact that the ligand-binding domain has a closed conformation (Safe, 2023). The activity of the transcription factor Nur77 is primarily regulated by its expression levels and posttranslational modifications. In macrophages, Nur77 protein has been described to localize to the nucleus (Pei et al., 2005). In our current study, we revealed that *Nur77* expression is significantly induced by LPS as shown with qPCR analysis and Nur77 deficiency affects the expression of mechanics-related genes. These findings suggest that Nur77 modulates macrophage mechanics primarily through its enhanced expression. As soon as other modes of regulation have been discovered, such as agonists or antagonists for Nur77, it would be interesting to modulate Nur77 activity and investigate the effect on macrophage inflammation and mechanics.

Taken together, we revealed that Nur77 acts as a key regulator of macrophage immunomechanics. The comparison of WT and Nur77-deficient macrophages revealed that the impact of Nur77 on cellular mechanics genes contributes to the overall function of this transcription factor in promoting the resolution of inflammation, modulation of migration, and phagocytosis in activated macrophages.

4. Methods

4.1. Experimental models and subject details

4.1.1. Mouse strains

All animal housing, care, and experimental procedures were conducted in accordance with the guidelines and regulations set forth by the Institutional Animal Experimental Committee for Animal Welfare, following the principles of Directive 2010/63/EU of the European Parliament. Whole-body Nur77 knockout mice were generated by crossing C57Bl6/J mice that overexpress Cre recombinase under the control of the human cytomegalovirus (CMV) promoter with mice harboring a loxP-flanked Nur77 (Nr4a1) locus (Koenis et al., 2018b). This breeding strategy allowed for the deletion of the Nur77 gene. The successful deletion of Nur77 was confirmed by genotyping PCR. Subsequently, Nur77-deficient mice that no longer expressed Cre recombinase were generated (referred to as Nur77-KO mice). Both Nur77-KO mice and their wild-type (WT) littermates were used in the experiments.

4.1.2. Bone marrow-derived macrophage (BMDM) differentiation and cell culture

Bone marrow cells were isolated from the femurs and tibias of male WT and Nur77-KO mice aged 6–12 weeks. The cells were differentiated into macrophages by culturing them in RPMI 1640 medium (Gibco, cat#22400089) supplemented with 10% fetal calf serum, 100 U/mL penicillin, 100 µg/mL streptomycin, 2 mM L-glutamine, 15% L929-conditioned medium, 1 mM sodium pyruvate, 1x MEM Non-Essential Amino Acids Solution (Gibco, cat#1140050), and 1x MEM Vitamin Solution (Gibco, cat#11120052) for a period of 7 days. BMDMs were seeded at a density of 1×10^6 cells per well in 6-well culture plates. After the differentiation process, the cells were lifted, counted, and re-seeded for further analyses. In all experiments involving LPS-stimulated BMDMs, a concentration of 100 ng/mL lipopolysaccharide (LPS) (Sigma, cat#L2637) was used. As a control for differentiation, we determined expression of differentiation markers CD11b+F4/80+ by flow cytometry and demonstrated that all cells were >99% positive for both markers (Toda et al., 2021).

4.2. Method details

4.2.1. Immunofluorescence microscopy

Differentiated BMDMs were seeded at a density of 0.5×10^5 cells per well on uncoated glass coverslips in a 24-well cell culture plate. The cells were stimulated with 100 ng/mL LPS (Sigma, cat#L2637) for 0, 6, 18, and 24 hours, followed by fixation with 4% paraformaldehyde (Sigma) in PBS for 10 minutes. After three washes with PBS, the cells were permeabilized with 0.5% Triton-X (Sigma)/PBS for 10 minutes and then blocked with 1% BSA/PBS for 30 minutes. The cells were first stained with DAPI (Invitrogen, cat#D21490) in 0.5% BSA/PBS for 15 minutes, followed by Alexa Fluor 568 Phalloidin (Invitrogen, cat#A12380) staining for 1 hour. Fluorescence images were acquired using the Leica SP8 confocal microscope.

4.2.2. AFS experimental setup

We reported details on the setup, specifications, and fabrication of AFS in previous papers (Evers et al., 2024, 2022, 2021). Briefly, all measurements were conducted on an AFS-G2 (Lumicks B.V., the Netherlands), which comprises a motorized z-stage mounted on an inverted microscope (Nikon Eclipse TE200), G2 AFS chip holders (microfluidic devices), and a temperature controller. Visualization and illumination were achieved by a motorized 20× microscope objective for a nanometer-precise z-translation, a red-light LED, and a uEye camera (UI-324xCP-M, IDS) capable of imaging with a sampling frequency of 60 Hz. The AFS chip consists of a microfluidic chamber for cell loading and a piezoelectric element on top to transduce the acoustic waves. Acoustic forces are applied on silica microspheres, which were tracked by image recording using LabVIEW (provided by Lumicks B.V.) for real-time, x, y, and z tracking of bead location.

4.2.3. AFS experiments

BMDM WT and Nur77-KO cell suspensions, at a density of 40×10^6 cells/mL mixed with silica microspheres (7.9 µm in diameter; Spherotech, SIP-60–10), were injected into the microfluidic chambers of the AFS chips before being placed into the incubator. Non-attached and dead cells were flushed out by connecting the AFS chip to a syringe pump (AL-2000, World Precision Instruments) after 2 h incubation, and BMDMs were cultured inside the incubator overnight at a slow flow rate (3 µl/min). WT and Nur77-KO macrophages were exposed to 100 ng/mL LPS (Sigma, cat#L2637) for 6 h while being cultured inside the AFS chip. On the day of measurement, each individual bead in the field of view was tracked by LabVIEW and their z-position was determined by a look-up-table (LUT), set to track from 0 to 10 000 nm at a step size of 100 nm. After calibration (for details see previous paper (Evers et al., 2022), a constant acoustic force (≈1.7 nN) was applied, pushing the beads upward, thereby stretching the macrophages. All measurements were performed at 37°C, with an amplitude of 30%-60% at 14.47 and 14.51 MHz frequency, and applied constantly for a period of 20 s.

4.3. Migration assay

Cell migration assays were performed using the µ-Slide Chemotaxis (80326, ibidi GmbH) according to the manufacturer's protocol. Briefly, BMDM cell suspensions (6 µL) of 3×10^6 cells/mL were seeded into the center chamber of a µ-Slide. After cell adhesion, the two opposing reservoirs were filled with culture medium containing 10% FCS. Cell migration was recorded every 10 min overnight by mounting the µ-Slide on the stage of a Nikon Eclipse Ti inverted microscope with a 37 °C incubator and 5% CO2. Single-cell tracking and analysis in the observation area of each image sequence was done using the Manual Tracking plugin of ImageJ and ibidi Chemotaxis and Migration Tool (version 2.0) which does not provide single cell quantification but averaged numbers.

4.4. Adhesion assay

After differentiation in 6-well plates, BMDMs were stimulated with 100 ng/mL LPS (Sigma, cat#L2637) for 20 hours. The cells were then washed with PBS and lifted with 4 mg/mL lidocaine hydrochloride (Supelco) for 5 minutes at 37°C. After centrifugation, 0.6×10^5 cells were plated on ICAM-1-coated (12,5 µg/mL; R&D systems, cat#796-IC) 96-well plates. The cells were allowed to attach for 30 minutes, followed by the removal of the media and replacement with warm HBSS containing 1:1000 Hoechst 34580 (Sigma, cat#63493). After an additional 30 minutes of incubation, the cells were fixed with 4% paraformaldehyde (Sigma) for 15 minutes. The cells were then washed and analyzed using the ImageXpress Pico with cell count analysis.

4.5. Phagocytosis assay

Differentiated BMDMs were seeded at a density of 0.6×10^5 cells per well in a 96-well cell culture plate. The following day, 1×10^6 Zymosan beads (Invitrogen, cat#Z23374) per well were washed and resuspended in PBS. The beads were added to the cells and incubated for 30 minutes at 37°C. After incubation, the cells were washed and incubated with fresh medium for another 30 minutes at 37°C. Subsequently, the cells were washed and lysed with RIPA buffer (50 mM Tris-HCl pH 7.4, 150 mM NaCl, 1% IGEPAL CA-630, 0.5% sodiumdeoxycholate, 0.1% SDS). The Zymosan signal in the cell lysate was analyzed at 594 nm using a CLARIOstar (BMG Labtech) per well. For each biological replicate at least 3 wells were measured. To account for differences in cell numbers, a BSA Protein Assay Kit was used for normalization.

4.6. Flow cytometry

After differentiation in 6-well plates, BMDMs were stimulated with 100 ng/mL LPS (Sigma, cat#L2637) for 24 hours. The cells were washed and scraped with FACS buffer (PBS + 2% FBS + 5 mM EDTA (Sigma)). After pelleting the cells, they were incubated in FACS buffer containing CD16/CD32 (1:500, eBioscience™, cat#14–0161–82) for 15 minutes at 4°C and then transferred to a 96-well V-bottom plate. The cells were then incubated with the antibodies F4/80 (Invitrogen, cat#12–4801–82, 1:100), CD11b (Invitrogen, cat#17–0112–82, 1:100), and CD18 (Biolegend, cat#101405,1:100) for 30 minutes at 4°C. After washing, the cells were resuspended in FACS buffer containing 7-AAD (Invitrogen, cat#A1310, 1 μg/mL) to exclude dead cells. Samples were analyzed by flow cytometry using BD Facs Canto II (BD Biosciences) and analyzed with FlowJo v10.5.3 software (FlowJo LLC).

4.7. RNA sequencing (RNA-seq)

After differentiation in 6-well plates, BMDMs were stimulated 100 ng/mL LPS (Sigma, cat#L2637) for 0, 4, and 18 hours. Following stimulation, RNA was extracted using the RNeasy Mini kit with an on-column DNase-treatment according to the manufacturer's instructions (Qiagen). RNA concentration was determined using a Qubit fluorometer (Qiagen), RNA quality was evaluated using an Agilent Bioanalyzer 2100 system (Agilent Technologies). Strand-specific libraries were generated using the KAPA mRNA HyperPrep kit according to the manufacturer's instructions. Libraries were pooled and diluted to 25 nM prior to sequencing on a Novaseq 6000 instrument (Illumina) at a depth of 20 million paired ended 150 base pair reads.

4.8. Reverse transcription (RT)-qPCR

Total RNA from differentiated and stimulated BMDMs was isolated using TRIreagent (Sigma) following the manufacturer's instructions. The RNA pellet was dried and dissolved in nuclease-free ultrapure water. The RNA concentration was determined using a Nanodrop UV–VIS Spectrophotometer. Reverse transcription was performed on 1 μg of RNA using the iScript cDNA Synthesis Kit (Bio-Rad). Quantitative PCR (qPCR) was carried out using the SensiFAST SYBR No-ROX kit (Bioline) on a LightCycler 480 II PCR platform (Roche). Primer set amplification efficiencies and transcript starting concentrations (N0) were calculated using LinRegPCR (Untergasser et al., 2021). Target gene expression was normalized by dividing it by the geometric mean of *Rplp0* and *Hrpt* housekeeping gene expression. The primer sequences used for RT-qPCR are Nur77-*TTGAGTTCGGCAAGCCTACC*, Rplp0-*GGACCCGAGAAGACCTCCTT*, Hprt-*TTGCTCGAGATGTCATGAAGGA*.

4.9. Western blotting

After differentiation in 6-well plates, BMDMs were stimulated with 100 ng/mL LPS (Sigma, cat#L2637) for 0, 4, and 18 hrs. Differentiated BMDMs were then washed with PBS and lysed in ice cold RIPA buffer (50 mM Tris-HCl pH 7.4, 150 mM NaCl, 1% IGEPAL CA-630, 0.5% sodiumdeoxycholate, 0.1% SDS) supplemented with protease inhibitor (cOmplete mini EDTA-free; Merck, cat#11836170001) and phosphatase inhibitor (PhosSTOP; Roche, PHOSS-RO). Protein quantification was performed using the DC Protein Assay Kit (Bio-Rad) following the manufacturer's protocol. Protein samples were heated for 5 min at 96°C. Total protein (15 μg) was separated on a 4–12% Bolt Bis-Tris gel (Invitrogen, cat#NW04120BOX) and transferred onto a nitrocellulose membrane (Bio-Rad). The membranes were blocked with 2% nonfat milk in 0.1% Tween (v/v) in PBS (TBS-T) for 1 hour and then incubated with rabbit-Itgb2 (Proteintech, cat#10554–1-AP) and rabbit-Capza2 (Proteintech, cat#15948–1-AP). After three washes with TBS-T, the protein bands were detected by incubating the membranes with horseradish peroxidase (HRP)-conjugated secondary antibodies for 1 hour at room temperature. Following five washes with TBS-T, the protein bands were visualized using the Supersignal West Pico PLUS chemiluminescent substrate (ThermoFisher, cat#34580) and captured with the Image-Quant 800 Western blot imaging system (Amersham).

4.10. Quantification and statistical analysis

4.10.1. Statistical Analysis

Statistical analysis was performed using GraphPad Prism 8.0.1., except the RNA-seq data which were analyzed in Rstudio. Data are shown as mean ± SEM, unless stated otherwise. Number of replicates (n) and the statistical tests used are indicated in the figure legends, with a p-value < 0.05 considered significant. Other levels of significance are reported as: *p<0.05;**p<0.01;***p<0.001;****p<0.0001. Normal data distribution was tested using Kolmogorov-Smirnov normality test. P values were calculated using a ratio/multiple paired t-test or a two-way ANOVA with either Bonferroni or Tukey post hoc correction as indicated in the figure legends.

4.11. Analysis of WT and Nur77 macrophage mechanical properties

The mechanical properties were determined by fitting to the standard linear liquid (SLL) model. The creep compliance J(t), as a function of time, in the SLL model is given by:

$$J(t) = \left(\frac{t}{\eta a + \eta c}\right) + \left(\frac{(\eta a)^2}{Ea(\eta a + \eta c)^2}\right) * \left(1 - e^{\left(\frac{-t}{\frac{\eta a * \eta c}{Ea(\eta a + \eta c)}}\right)}\right) \quad (1)$$

where Ea is the elastic modulus associated with the actin cytoskeleton, ηa the viscous contribution of the cytoskeleton, and ηc the background viscosity.

The extension curves, z-height versus time, were first converted to J (t), where,

$$J(t) = \frac{z(t)}{F} \times \pi r \quad (2)$$

Where z(t) is the extension curve (z-direction) obtained by pulling on a cell, F is the applied force, and r is the radius of the silica bead. J(t) was then plotted as a function of time and Eq. (1) was fit to the resultant curves. Three biological replicates were analyzed simultaneously and a Mann-Whitney test was used due to skewed data.

4.12. Quantification of RNA-seq

Reads were aligned to the mouse genome mm10 using HISAT2 2.1.0 (PMID: 31375807) with default settings. BAM files were indexed and filtered on MAPQ > 15 with SAMtools 1.16.1 (PMID: 33590861). Raw tag counts and RPKM (reads per kilo base per million mapped reads) values per gene were summed using HOMER2's analyzeRepeats.pl script with default settings and the -noadj or -rpkm options for raw counts and RPKM reporting, respectively. Differential expression was assessed using the DESeq2 Bioconductor package in an R 4.2.2 environment with a Benjamini-Hochberg adjusted P value < 0.05 and an average RPKM > 1 in at least one group. Genes with a false discovery rate (FDR)-adjusted p value < 0.05 and a log2 fold-change < -1 or > 1 were considered to be differentially regulated. To identify deregulated pathways the software packages Metascape (Zhou et al., 2019) and EGSEA (Alhamdoosh et al., 2017) were used.

4.13. Quantification of Images

The cell size analysis was performed with Icy image analysis

software,with which single cells per image were identified based on DAPI-stained nuclei by HK-means method (Dufour et al., 2008). To quantify cell size, the plug-in Active Countours was used, to generate precise ROIs for every cell (Dufour et al., 2011). Next, these ROIs were quantified to extract the area of the cell. This was done for multiple field of views per coverslip. Multiple coverslips per mice were analyzed with n=number of mice.

Quantification of ruffled edges was performed in ImageJ by using previously published protocol (Kreider-Letterman et al., 2022). An average per field of view is calculated, this was done for multiple field of views (at least 5) per mice with n=number of mice.

Data resources

The accession number is for the raw and processed RNA-seq data reported in this paper is GEO: GSE253423

CRediT authorship contribution statement

Sanne C. Lith: Writing – original draft, Investigation, Conceptualization. **Carlie J.M. de Vries:** Writing – review & editing, Writing – original draft, Conceptualization. **Winnie G. Vos:** Investigation. **Tom M.J. Evers:** Writing – original draft, Investigation, Conceptualization. **Beatriz M. Freire:** Investigation. **Claudia M. van Tiel:** Investigation. **Alireza Mashaghi:** Writing – review & editing, Funding acquisition, Conceptualization.

Declaration of Competing Interest

The authors declare that they have no known competing financial interests or personal relationships that could have appeared to influence the work reported in this paper.

Acknowledgments

We thank Marten Hoeksema for the discussion. A.M. and T.M.J.E. acknowledge this work was supported by the Nederlandse Organisatie voor Wetenschappelijk Onderzoek [grant number OCENW.XS22.4.185, OCENW.XS23.3.105]. B.M.F. acknowledges this work was supported by the FAPESP grant [grant number 2017/2624–1, 2021/11220–8].

Appendix A. Supporting information

Supplementary data associated with this article can be found in the online version at doi:10.1016/j.ejcb.2024.151419.

References

Alhamdoosh, M., Ng, M., Wilson, N.J., Sheridan, J.M., Huynh, H., Wilson, M.J., Ritchie, M.E., 2017. Combining multiple tools outperforms individual methods in gene set enrichment analyses. Bioinformatics 33, 414–424. https://doi.org/10.1093/bioinformatics/btw623.

Allen, W.E., Jones, G.E., Pollard, J.W., Ridley, A.J., 1997. Rho, Rac and Cdc42 regulate actin organization and cell adhesion in macrophages. J. Cell Sci. 110, 707–720. https://doi.org/10.1242/JCS.110.6.707.

Atcha, H., Meli, V.S., Davis, C.T., Brumm, K.T., Anis, S., Chin, J., Jiang, K., Pathak, M.M., Liu, W.F., 2021. Crosstalk between CD11b and Piezo1 Mediates Macrophage Responses to Mechanical Cues. Front Immunol. 12, 1–14. https://doi.org/10.3389/fimmu.2021.689397.

Bonta, P.I., van Tiel, C.M., Vos, M., Pols, T.W.H., van Thienen, J.V., Ferreira, V., Arkenbout, E.K., Seppen, J., Spek, C.A., van der Poll, T., Pannekoek, H., de Vries, C.J. M., 2006. Nuclear receptors Nur77, Nurr1, and NOR-1 expressed in atherosclerotic lesion macrophages reduce lipid loading and inflammatory responses. Arterioscler. Thromb. Vasc. Biol. 26, 2288–2294. https://doi.org/10.1161/01.ATV.0000238346.84458.5d.

Bouti, P., Webbers, S.D.S., Fagerholm, S.C., Alon, R., Moser, M., Matlung, H.L., Kuijpers, T.W., 2021. β 2 integrin signaling cascade in neutrophils: more than a single function. Front Immunol. 11 https://doi.org/10.3389/FIMMU.2020.619925.

Bufi, N., Saitakis, M., Dogniaux, S., Buschinger, O., Bohineust, A., Richert, A., Maurin, M., Hivroz, C., Asnacios, A., 2015. Human primary immune cells exhibit distinct mechanical properties that are modified by inflammation. Biophys. J. 108, 2181–2190. https://doi.org/10.1016/j.bpj.2015.03.047.

Chen, M., Zhang, Y., Zhou, P., Liu, X., Zhao, H., Zhou, X., Gu, Q., Li, B., Zhu, X., Shi, Q., 2020. Substrate stiffness modulates bone marrow-derived macrophage polarization through NF-κB signaling pathway. Bioact. Mater. 5, 880–890. https://doi.org/10.1016/j.bioactmat.2020.05.004.

Chianese, U., Papulino, C., Passaro, E., Evers, T.M., Babaei, M., Toraldo, A., De Marchi, T., Niméus, E., Carafa, V., Nicoletti, M.M., Del Gaudio, N., Iaccarino, N., Randazzo, A., Rotili, D., Mai, A., Cappabianca, S., Mashaghi, A., Ciardiello, F., Altucci, L., Benedetti, R., 2022. Histone lysine demethylase inhibition reprograms prostate cancer metabolism and mechanics. Mol. Metab. 64, 101561 https://doi.org/10.1016/J.MOLMET.2022.101561.

Condon, N., Stow, J., Wall, A., 2020. Automated analysis of cell surface ruffling: ruffle quantification macro. Bio Protoc. 10, 1–12. https://doi.org/10.21769/bioprotoc.3494.

De Waard, V., Arkenbout, E.K., Vos, M., Mocking, A.I.M., Niessen, H.W.M., Stooker, W., De Mol, B.A.J.M., Quax, P.H.A., Bakker, E.N.T.P., VanBavel, E., Pannekoek, H., De Vries, C.J.M., 2006. TR3 nuclear orphan receptor prevents cyclic stretch-induced proliferation of venous smooth muscle cells. Am. J. Pathol. 168, 2027–2035. https://doi.org/10.2353/AJPATH.2006.050932.

Dufour, A., Meas-Yedid, V., Grassart, A., Olivo-Marin, J.C., 2008. Automated quantification of cell endocytosis using active contours and wavelets. Proc. - Int. Conf. Pattern Recognit. https://doi.org/10.1109/ICPR.2008.4761748.

Dufour, A., Thibeaux, R., Labruyère, E., Guillén, N., Olivo-Marin, J.C., 2011. 3-D active meshes: fast discrete deformable models for cell tracking in 3-D time-lapse microscopy. IEEE Trans. Image Process. 20, 1925–1937. https://doi.org/10.1109/TIP.2010.2099125.

Dupuy, A.G., Caron, E., 2008. Integrin-dependent phagocytosis - spreading from microadhesion to new concepts. J. Cell Sci. 121, 1773–1783. https://doi.org/10.1242/jcs.018036.

Dutta, B., Goswami, R., Rahaman, S.O., 2020. TRPV4 plays a role in matrix stiffness-induced macrophage polarization. Front Immunol. 11, 1–12. https://doi.org/10.3389/fimmu.2020.570195.

Evers, T.M.J., Babaei, M., Mashaghi, A., 2024. Probing human immune cell mechanics using acoustic force spectroscopy. STAR Protoc. 5 https://doi.org/10.1016/J.XPRO.2024.102861.

Evers, T.M.J., Sheikhhassani, V., Haks, M.C., Storm, C., Ottenhoff, T.H.M., Mashaghi, A., 2021. Single-cell analysis reveals chemokine-mediated differential regulation of monocyte mechanics. iScience 25. https://doi.org/10.1016/J.ISCI.2021.103555.

Evers, T.M.J., Sheikhhassani, V., Tang, H., Haks, M.C., Ottenhoff, T.H.M., Mashaghi, A., 2022. Single-cell mechanical characterization of human macrophages. Adv. Nanobiomed Res 2. https://doi.org/10.1002/ANBR.202100133.

Glass, C.K., Natoli, G., 2015. Molecular control of activation and priming in macrophages, 17 Nat. Immunol. 2015 17 (1), 26–33. https://doi.org/10.1038/ni.3306.

Hamers, A.A.J., Argmann, C., Moerland, P.D., Koenis, D.S., Marinković, G., Sokolović, M., de Vos, A.F., de Vries, C.J.M., van Tiel, C.M., 2016. Nur77-deficiency in bone marrow-derived macrophages modulates inflammatory responses, extracellular matrix homeostasis, phagocytosis and tolerance. BMC Genom. 17, 162. https://doi.org/10.1186/s12864-016-2469-9.

Hamers, A.A.J., Vos, M., Rassam, F., Marinković, G., Kurakula, K., van Gorp, P.J., de Winther, M.P.J., Gijbels, M.J.J., de Waard, V., de Vries, C.J.M., 2012. Bone marrow–specific deficiency of nuclear receptor Nur77 enhances atherosclerosis. Circ. Res. 110, 428–438. https://doi.org/10.1161/CIRCRESAHA.111.260760.

Hanna, R.N., Carlin, L.M., Hubbeling, H.G., Nackiewicz, D., Green, A.M., Punt, J.A., Geissmann, F., Hedrick, C.C., 2011. The transcription factor NR4A1 (Nur77) controls bone marrow differentiation and the survival of Ly6C- monocytes. Nat. Immunol. 12, 778–785. https://doi.org/10.1038/ni.2063.

Hanna, R.N., Shaked, I., Hubbeling, H.G., Punt, J.A., Wu, R., Herrley, E., Zaugg, C., Pei, H., Geissmann, F., Ley, K., Hedrick, C.C., 2012. NR4A1 (Nur77) deletion polarizes macrophages toward an inflammatory phenotype and increases atherosclerosis. Circ. Res 110, 416–427. https://doi.org/10.1161/CIRCRESAHA.111.253377.

Hu, Y.-W., Zhang, P., Yang, J.-Y., Huang, J.-L., Ma, X., Li, S.-F., Zhao, J.-Y., Hu, Y.-R., Wang, Y.-C., Gao, J.-J., Sha, Y.-H., Zheng, L., Wang, Q., 2014. Nur77 decreases atherosclerosis progression in apoE−/− mice fed a high-fat/high-cholesterol diet. PLoS One 9, e87313. https://doi.org/10.1371/journal.pone.0087313.

Jain, N., Moeller, J., Vogel, V., 2019. Mechanobiology of macrophages: how physical factors coregulate macrophage plasticity and phagocytosis. Annu Rev. Biomed. Eng. 21, 267–297. https://doi.org/10.1146/annurev-bioeng-062117-121224.

Koenis, D.S., Medzikovic, L., van Loenen, P.B., van Weeghel, M., Huveneers, S., Vos, M., Evers-van Gogh, I.J., Van den Bossche, J., Speijer, D., Kim, Y., Wessels, L., Zelcer, N., Zwart, W., Kalkhoven, E., de Vries, C.J., 2018a. Nuclear receptor Nur77 limits the macrophage inflammatory response through transcriptional reprogramming of mitochondrial metabolism. Cell Rep. 24, 2127. https://doi.org/10.1016/J.CELREP.2018.07.065.

Koenis, D.S., Medzikovic, L., Vos, M., Beldman, T.J., Van Loenen, P.B., Van Tiel, C.M., Hamers, A.A.J., Rubio, I.O., De Waard, V., De Vries, C.J.M., 2018b. Nur77 variants solely comprising the amino-terminal domain activate hypoxia-inducible factor-1 α and affect bone marrow homeostasis in mice and humans. J. Biol. Chem. 293, 15070–15083. https://doi.org/10.1074/jbc.RA118.002720.

Kreider-Letterman, G., Cooke, M., Goicoechea, S.M., Kazanietz, M.G., Garcia-Mata, R., 2022. Quantification of ruffle area and dynamics in live or fixed lung adenocarcinoma cells. STAR Protoc. 3, 101437 https://doi.org/10.1016/J.XPRO.2022.101437.

Li, L., Liu, Y., Chen, H., Li, F., Wu, J., Zhang, H., He, J., Xing, Y., Chen, Y., Wang, W., Tian, X., Li, A., Zhang, Q., Huang, P., Han, J., Lin, T., Wu, Q., 2015. Impeding the interaction between Nur77 and p38 reduces LPS-induced inflammation. Nat. Chem. Biol. 11, 339–346. https://doi.org/10.1038/nchembio.1788.

Liddiard, K., Taylor, P.R., 2015. Understanding local macrophage phenotypes in disease: shape-shifting macrophages, 21 Nat. Med. 2015 21 (2), 119–120. https://doi.org/10.1038/nm.3798.

Lith, S.C., de Vries, C.J.M., 2021. Nuclear receptor Nur77: Its role in chronic inflammatory diseases. Essays Biochem 65, 927–939. https://doi.org/10.1042/EBC20210004.

Liu, H., Zhu, L., Dudiki, T., Gabanic, B., Good, L., Podrez, E.A., Cherepanova, O.A., Qin, J., Byzova, T.V., 2020. Macrophage migration and phagocytosis are controlled by Kindlin-3's Link to the Cytoskeleton. J. Immunol. 204, 1954–1967. https://doi.org/10.4049/jimmunol.1901134.

Mao, Y., Finnemann, S.C., 2015. Regulation of phagocytosis by Rho GTPases. https://doi.org/10.4161/21541248.2014.989785.

Mcwhorter, F.Y., Davis, C.T., Liu, W.F., Hall, E., Irvine, C., 2016. Physical and mechanical regulation of macrophage phenotype and function 72, 1303–1316. https://doi.org/10.1007/s00018-014-1796-8.Physical.

Medrano-Bosch, M., Simón-Codina, B., Jiménez, W., Edelman, E.R., Melgar-Lesmes, P., 2023. Monocyte-endothelial cell interactions in vascular and tissue remodeling. Front Immunol. 14, 1196033. https://doi.org/10.3389/FIMMU.2023.1196033/BIBTEX.

Morrison, V.L., James, M.J., Grzes, K., Cook, P., Glass, D.G., Savinko, T., Lek, H.S., Gawden-Bone, C., Watts, C., Millington, O.R., MacDonald, A.S., Fagerholm, S.C., 2014. Loss of beta2-integrin-mediated cytoskeletal linkage reprogrammes dendritic cells to a mature migratory phenotype, 5 Nat. Commun. 2014 5 (1), 1–13. https://doi.org/10.1038/ncomms6359.

Mukhopadhyay, M., 2023. Immunomechanics. Nat. Methods 2023 20 (1), 35. https://doi.org/10.1038/s41592-022-01739-1. -35.

Okamoto, T., Takagi, Y., Kawamoto, E., Park, E.J., Usuda, H., Wada, K., Shimaoka, M., 2018. Reduced substrate stiffness promotes M2-like macrophage activation and enhances peroxisome proliferator-activated receptor γ expression. Exp. Cell Res 367, 264–273. https://doi.org/10.1016/j.yexcr.2018.04.005.

Patel, N.R., Bole, M., Chen, C., Hardin, C.C., Kho, A.T., Mih, J., Deng, L., Butler, J., Tschumperlin, D., Fredberg, J.J., Krishnan, R., Koziel, H., 2012. Cell elasticity determines macrophage function. PLoS One 7, 1–10. https://doi.org/10.1371/journal.pone.0041024.

Pei, L., Castrillo, A., Chen, M., Hoffmann, A., Tontonoz, P., 2005. Induction of NR4A orphan nuclear receptor expression in macrophages in response to inflammatory stimuli. J. Biol. Chem. 280, 29256–29262. https://doi.org/10.1074/jbc.M502606200.

Ronzier, E., Laurenson, A.J., Manickam, R., Liu, S., Saintilma, I.M., Schrock, D.C., Hammer, J.A., Rotty, J.D., 2022. The actin cytoskeleton responds to inflammatory cues and alters macrophage activation. Cells 11. https://doi.org/10.3390/CELLS11111806/S1.

Ross, G.D., Vetvicka, V., 1993. CR3 (CDllb, CD18): a phagocyte and NK cell membrane receptor with multiple ligand specificities and functions. Clin. Exp. Immunol. 92, 181–184.

Rotty, J.D., Brighton, H.E., Craig, S.L., Asokan, S.B., Cheng, N., Ting, J.P., Bear, J.E., 2017. Arp2/3 complex is required for macrophage integrin functions but is dispensable for FcR phagocytosis and in vivo motility. Dev. Cell 42, 498. https://doi.org/10.1016/J.DEVCEL.2017.08.003.

Ruoslahti, E., 1991. Integrins. J. Clin. Investig. 87, 1–5. https://doi.org/10.1172/JCI114957.

Safe, S., 2023. Natural products and synthetic analogs as selective orphan nuclear receptor 4A (NR4A) modulators. Histol. Histopathol. 18689. https://doi.org/10.14670/HH-18-689.

Schittenhelm, L., Hilkens, C.M., Morrison, V.L., 2017. B2 integrins as regulators of dendritic cell, monocyte, and macrophage function. Front Immunol. 8 https://doi.org/10.3389/fimmu.2017.01866.

Shaked, I., Hanna, R.N., Shaked, H., Chodaczek, G., Nowyhed, H.N., Tweet, G., Tacke, R., Basat, A.B., Mikulski, Z., Togher, S., Miller, J., Blatchley, A., Salek-Ardakani, S., Darvas, M., Kaikkonen, M.U., Thomas, G.D., Lai-Wing-Sun, S., Rezk, A., Bar-Or, A., Glass, C.K., Bandukwala, H., Hedrick, C.C., 2015. Transcription factor Nr4a1 couples sympathetic and inflammatory cues in CNS-recruited macrophages to limit neuroinflammation. Nat. Immunol. 16, 1228–1234. https://doi.org/10.1038/ni.3321.

Sun, H., Zhi, K., Hu, L., Fan, Z., 2021. The activation and regulation of β2 integrins in phagocytes and phagocytosis. Front Immunol. 12, 1–11. https://doi.org/10.3389/fimmu.2021.633639.

Toda, G., Yamauchi, T., Kadowaki, T., Ueki, K., 2021. Preparation and culture of bone marrow-derived macrophages from mice for functional analysis. STAR Protoc. 2 https://doi.org/10.1016/J.XPRO.2020.100246.

Underhill, D.M., Ozinsky, A., 2002. Phagocytosis of microbes: complexity in action. Annu Rev. Immunol. 20, 825–852. https://doi.org/10.1146/ANNUREV.IMMUNOL.20.103001.114744.

Untergasser, A., Ruijter, J.M., Benes, V., van den Hoff, M.J.B., 2021. Web-based LinRegPCR: application for the visualization and analysis of (RT)-qPCR amplification and melting data. BMC Bioinforma. 22 https://doi.org/10.1186/S12859-021-04306-1.

Wu, H., Li, X.-M., Wang, J.-R., Gan, W.-J., Jiang, F.-Q., Liu, Y., Zhang, X.-D., He, X.-S., Zhao, Y.-Y., Lu, X.-X., Guo, Y.-B., Zhang, X.-K., Li, J.-M., 2016. NUR77 exerts a protective effect against inflammatory bowel disease by negatively regulating the TRAF6/TLR-IL-1R signalling axis. J. Pathol. 238, 457–469. https://doi.org/10.1002/path.4670.

Zhou, Y., Zhou, B., Pache, L., Chang, M., Khodabakhshi, A.H., Tanaseichuk, O., Benner, C., Chanda, S.K., 2019. Metascape provides a biologist-oriented resource for the analysis of systems-level datasets. Nat. Commun. 10 https://doi.org/10.1038/S41467-019-09234-6.